Hindawi Publishing Corporation
Journal of Biomedicine and Biotechnology
Volume 2011, Article ID 267206, 9 pages
doi:10.1155/2011/267206

Research Article

Development of ^{68}Ga-Glycopeptide as an Imaging Probe for Tumor Angiogenesis

Ning Tsao,[1] Chau-Hui Wang,[2] Li-Jane Her,[3] Kai-Yuan Tzen,[4] Jing-Yi Chen,[2] Dong-Fang Yu,[1] and David J. Yang[1]

[1] *Division of Diagnostic Imaging, University of Texas MD Anderson Cancer Center, 1515 Holcombe Boulevard, Houston, TX 77030, USA*
[2] *Chemistry, Manufacturing and Control, SeeCure LLC, Houston, TX 77036, USA*
[3] *Innovation Center, Taiwan HOPAX Chems, MFG, Company Ltd., Kaohsiung 831, Taiwan*
[4] *Department of Nuclear Medicine, National Taiwan University Hospital, Taipei 100, Taiwan*

Correspondence should be addressed to Ning Tsao, ning.tsao@mdanderson.org

Received 28 December 2010; Accepted 15 February 2011

Academic Editor: Lie-Hang Shen

Objective. This study was aimed to study tissue distribution and tumor imaging potential of ^{68}Ga-glycopeptide (GP) in tumor-bearing rodents by PET. *Methods*. GP was synthesized by conjugating glutamate peptide and chitosan. GP was labeled with ^{68}Ga chloride for in vitro and in vivo studies. Computer outlined region of interest (counts per pixel) of the tumor and muscle (at the symmetric site) was used to determine tumor-to-muscle count density ratios. To ascertain the feasibility of ^{68}Ga-GP in tumor imaging in large animals, PET/CT imaging of ^{68}Ga-GP and ^{18}F-FDG were conducted in New Zealand white rabbits bearing VX2 tumors. Standard uptake value of tumors were determined by PET up to 45 min. To determine blood clearance and half-life of ^{68}Ga-GP, blood samples were collected from 10 seconds to 20 min. *Results*. Radiochemical purity of ^{68}Ga-GP determined by instant thin-layer chromatography was >95%. Tumor uptake values (SUV) for ^{68}Ga-GP and ^{18}F-FDG in New Zealand white rabbits bearing VX2 tumors were 3.25 versus 7.04. PET images in tumor-bearing rats and rabbits confirmed that ^{68}Ga-GP could assess tumor uptake. From blood clearance curve, the half-life of ^{68}Ga-GP was 1.84 hr. *Conclusion* Our data indicate that it is feasible to use ^{68}Ga-GP to assess tumor angiogenesis.

1. Introduction

With progress of molecular biology in recent years, imaging techniques are undergoing tremendous development and improvement. These imaging modalities play a major role in the development of novel therapies, since they generate information about target expression as well as function, pathway activity, and cell migration in the intact organism. For instance, angiogenesis, the proliferation of endothelial and smooth muscle cells to form new blood vessels, is an essential component of the metastatic pathway. These vessels provide the principal route by which tumor cells exit the primary tumor site and enter the circulation. For many tumors, the vascular density can provide a prognostic indicator of metastatic potential, with the highly vascular tumors having a higher incidence of metastasis than poorly vascular tumors [1]. Experimental research suggests that it is possible to block angiogenesis by specific inhibitory agents, and that modulation of angiogenic activity is associated with tumor regression in animals with different types of neoplasia. The promising angiosuppressive agents for clinical testing are naturally occurring inhibitors of angiogenesis (angiostatin, endostatin, platelet factor-4, and others). Measuring angiogenesis (blood vessel density) and/or its main regulators such as vascular endothelial growth factor (VEGF) and basic fibroblast growth factor (bFGF), or the levels of apoptosis after treatment in solid tumors provides new and sensitive markers for tumor progression, metastasis, and prognosis [2, 3].

Polysaccharides such as heparin, chitosan, and chondroitin play a potent role in tumor growth, tissue repair, and angiogenesis. Chitosan, an angiogenesis biomer, interacts

with vascular endothelia cells and potentiates the fibroblast growth factor (FGF-2) activity. Chitosan is known as a wound-dressing and tissue-adhesive material showing biocompatibility, anti-infective activity, and the ability to accelerate wound healing [4–6]. During the healing process, chitosan enhances macrophage activation, cytokine (IL-8) production by macrophages and fibroblasts, anti-inflammatory action, angiogenesis stimulation, granulation, and scar formation. Though chitosan has made outstanding advantage in the field of angiogenesis, some significant limitations still remain in the treatment of cancer via intracellular delivery of cytotoxic drugs. In order to enhance therapeutic index of chitosan in cancer treatment, we conjugated glutamate peptide with chitosan.

The excitatory amino acid glutamate (Glu) is a potent neurotransmitter in the central nervous system and exerts its action via a variety of glutamate transporters [7]. It is known that cellular uptake of polyglutamate peptide (GAP) is specific to glutamate transporter [8]. Chain of 5 or more glutamic acids could reduce renal uptake in animal models [9]. Conjugation of GAP with chitosan resulting in GP would be a novel agent to target tumor vascular and cellular component. Radiolabeled GP would support this concept.

Imaging science enables the comprehensive characterization of therapeutic intervention and can be used in preclinical studies, pharmacokinetic studies, dose-finding studies, and proof-of-concept studies. Positron emission tomography (PET) and single photon emission computed tomography (SPECT) permit mapping and measuring the rate of physiological, biochemical, and molecular processes with radiolabeled compounds and appropriate tracer kinetic models. Cellular imaging by PET and SPECT provides valuable information in monitoring and guiding clinical trial using cell-based therapies in the treatment of malignant and other diseases. ^{68}Ga and ^{99m}Tc are the most attractive radiometals obtained from generators for PET and SPECT clinical applications due to their energy (511 and 140 keV), half-life (68 min and 6 h), and simple coordination chemistry. We previously have reported that glycopeptide (GP), a copolymer of chitosan and glutamate peptide, provides an opportunity to target tumor vasculature and cellular via glutamate transporters [10]. In vitro assays revealed that cell uptake of ^{99m}Tc-GP was via glutamate transporters. ^{99m}Tc-GP was able to measure tumor uptake changes after paclitaxel treatment. Biodistribution of ^{99m}Tc-GP showed increased tumor-to-tissue count density ratios as a function of time. Planar images confirmed that it is feasible to use ^{99m}Tc-GP to assess tumor angiogenesis. To evaluate whether GP could also be labeled with a different isotope for PET imaging of tumors, here, we report the tissue distribution and tumor imaging potential of ^{68}Ga-GP.

2. Materials and Methods

2.1. Synthesis of ^{68}Ga-Glycopeptide (GP). To a stirred solution of chitosan (200 mg, MW 3,500–5,000) in water (4 mL) and 3-ethyl-3-(3-dimethylaminopropyl) carbodiimide-HCl (EDC) (128.5 mg, 0.67 mmoL) (Pierce Chemical Company, Rockford, IL) was added. Glutamate peptide sodium salt (200 mg, MW 1,308) was then added. The mixture was stirred at room temperature for 24 hr. The mixture was dialyzed for 48 hr using Spectra/POR molecular porous membrane with cutoff at 5,000 (Spectrum Medical Industries Inc., Houston, TX). After dialysis, the product was filtered and dried using a freeze dryer (Labconco, Kansas City, MO). The GP in the salt form weighed 320 mg. The chemical structure is shown in Figure 1. Gel permeation chromatogram (GPC) and capillary electrophoresis (CE) were used to analyze the purity of GP.

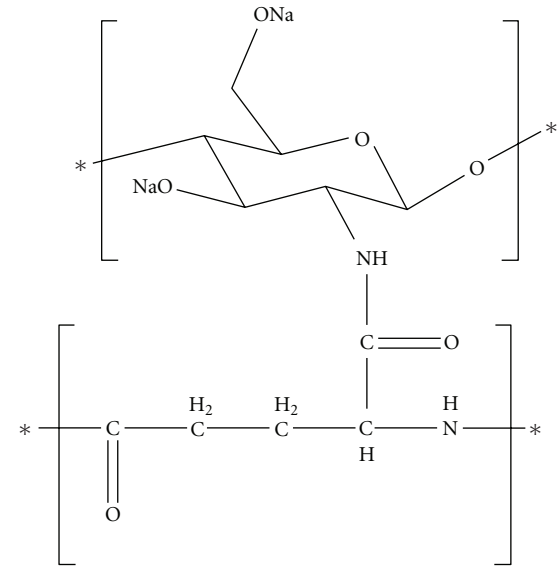

Figure 1: Structure of glycopeptide (GP).

Table 1: Biodistribution of ^{68}Ga-GP in breast tumor-bearing Rats. % of injected dose per gram of tissue weight (n = 3/time, interval, iv)*.

	30 min	60 min	120 min
Blood	2.61 ± 0.18	1.81 ± 0.05	1.37 ± 0.05
Heart	0.59 ± 0.06	0.43 ± 0.02	0.32 ± 0.02
Lung	2.34 ± 0.45	2.58 ± 0.16	1.38 ± 0.06
Thyroid	1.10 ± 0.11	1.40 ± 0.87	0.59 ± 0.06
Pancreas	0.38 ± 0.03	0.34 ± 0.04	0.28 ± 0.02
Liver	3.81 ± 0.32	4.83 ± 0.54	4.94 ± 0.38
Spleen	2.13 ± 0.07	2.65 ± 0.14	2.97 ± 0.11
Kidney	1.35 ± 0.02	1.36 ± 0.01	1.41 ± 0.11
Stomach	0.58 ± 0.04	0.65 ± 0.07	0.74 ± 0.18
Intestine	0.54 ± 0.12	0.53 ± 0.07	0.78 ± 0.22
Uterus	0.70 ± 0.02	0.65 ± 0.05	0.57 ± 0.03
Tumor	0.68 ± 0.12	0.89 ± 0.10	1.18 ± 0.09
Muscle	0.12 ± 0.02	0.12 ± 0.00	0.10 ± 0.02
Bone	0.45 ± 0.12	0.46 ± 0.09	0.59 ± 0.03
Brain	0.08 ± 0.01	0.07 ± 0.01	0.07 ± 0.01
Tumor/blood	0.26 ± 0.03	0.49 ± 0.07	0.86 ± 0.09
Tumor/muscle	6.12 ± 1.87	7.20 ± 0.83	13.26 ± 4.41

*Value shown represent the mean ± standard deviation of data from 3 animals at (Count at 460–560 keV window).

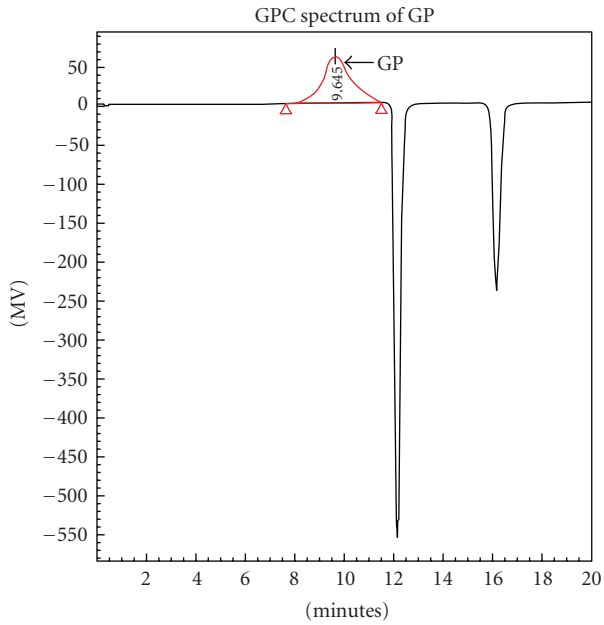

(a)

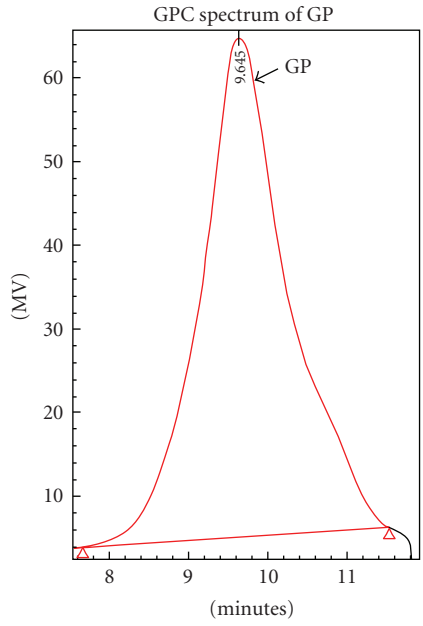

(b)

Figure 2: Gel permeation chromatogram (GPC) analysis of GP showed the purity of GP was greater than 95%. The spectrum showed the retention time of 9.645 min and the estimated molecular weight of 7,484.

2.2. Radiolabeling of GP with ^{68}Ga. Radiolabeling of GP with ^{68}Ga was performed in a standard manner [11]; briefly, GP (5 mg) was dissolved in 0.2 ml of water, and ^{68}Ga chloride (5 mCi) evaporated to dryness and reconstituted in 0.1 ml of sterilized water at room temperature, followed by heating up to 55°C for 10 min. Radiochemical purity was determined by instant thin-layer chromatography (ITLC Silica-Gel coated, Gelman Sciences, Ann Arbor, MI) eluted with saline.

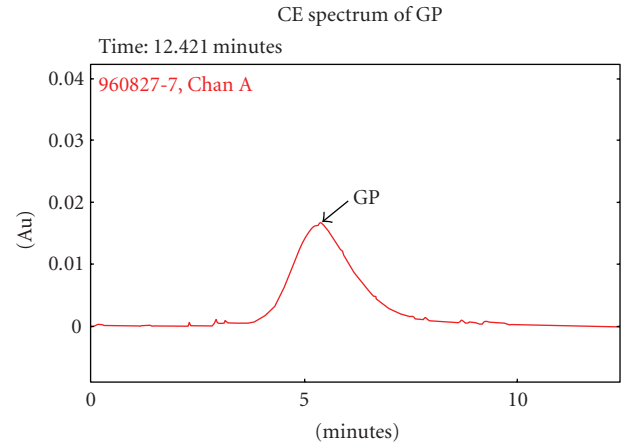

Figure 3: Capillary electrophoresis (CE) analysis of GP. The spectra showed that the purity of GP was greater than 95%.

Table 2: Biodistribution of FDG in breast tumor-bearing rats. % of injected dose per gram of tissue weight (n = 3/time, interval, i.v.)*.

	30 min	60 min	120 min
Blood	0.40 ± 0.04	0.13 ± 0.01	0.06 ± 0.00
Heart	1.57 ± 0.06	1.38 ± 0.13	1.08 ± 0.07
Lung	0.55 ± 0.06	0.42 ± 0.02	0.46 ± 0.03
Thyroid	1.07 ± 0.08	1.04 ± 0.04	1.05 ± 0.07
Pancreas	0.26 ± 0.03	0.21 ± 0.01	0.20 ± 0.02
Liver	0.40 ± 0.05	0.16 ± 0.01	0.13 ± 0.01
Spleen	0.82 ± 0.08	0.74 ± 0.03	0.86 ± 0.07
Kidney	0.71 ± 0.05	0.37 ± 0.01	0.24 ± 0.02
Stomach	0.61 ± 0.08	0.44 ± 0.03	0.39 ± 0.03
Intestine	0.69 ± 0.07	0.53 ± 0.03	0.52 ± 0.02
Uterus	0.51 ± 0.04	0.42 ± 0.03	0.41 ± 0.03
Tumor	2.13 ± 0.11	2.49 ± 0.08	2.03 ± 0.18
Muscle	0.33 ± 0.04	0.34 ± 0.03	0.74 ± 0.02
Bone	0.33 ± 0.04	0.44 ± 0.06	0.50 ± 0.03
Brain	2.00 ± 0.15	1.99 ± 0.05	1.39 ± 0.09
Tumor/blood	5.19 ± 0.38	19.78 ± 1.37	34.37 ± 1.76
Tumor/muscle	5.88 ± 0.57	7.54 ± 0.56	2.87 ± 0.24

*Value shown represent the mean ± standard deviation of data from 3 animals at (Count at 460–560 keV window).

2.3. In Vitro Stability Assays of ^{68}Ga-GP. ^{68}Ga-GP was prepared in the concentration of 5 mg/1 mCi/ml. 0.1 mL of ^{68}Ga-GP was incubated with 0.1 mL phosphate buffered saline (pH = 7.4) at 37°C for 30–120 min. In vitro stability of ^{68}Ga-GP was determined by chromatographic analysis, as described in the above section. There was no breakdown of ^{68}Ga-GP up to 2 hr.

2.4. Biodistribution Studies. Female Fischer 344 rats (150–175 g) (Harlan Sprague-Dawley, Inc., Indianapolis, IN) were inoculated subcutaneously in the right leg with breast cancer cells (10^6 cells in 0.1 mL/rat) from the 13762 cell line (known as DMBA-induced breast cancer cell line). Biodistribution studies were performed on day 14 after inoculation.

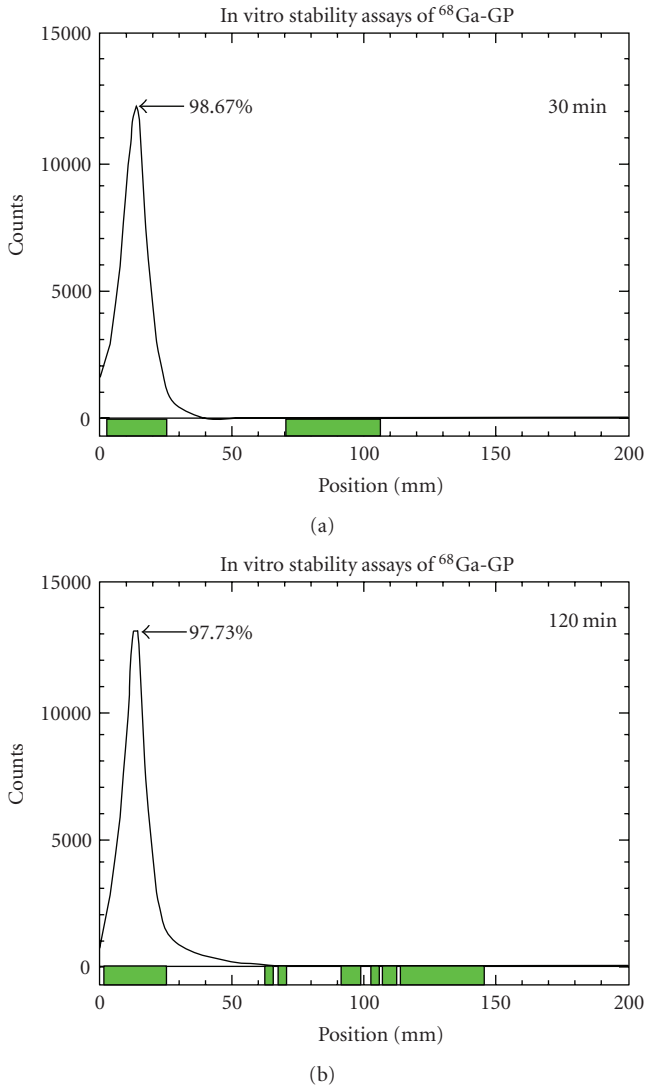

Figure 4: ^{68}Ga-GP was prepared in the concentration of 5 mg/1 mCi/1 mL. 0.1 mL of ^{68}Ga-GP was incubated with 0.1 mL phosphate buffered saline (pH = 7.4) at 30–120 min. There was no breakdown of ^{68}Ga-GP up to 120 min.

A group of Female Fischer 344 tumor-bearing rats was injected intravenously with ^{68}Ga-GP or ^{18}F-FDG (30 μCi/rat, $n = 3$ rats/time point) through the tail vein. The injected mass was 30 μg of ^{68}Ga-GP per rat. At 30, 60, and 120 min following administration of the radiotracers, the animals were sacrificed, and the tumor and selected tissues were excised, weighed, and counted for radioactivity with a gamma counter (Packard Instruments, Downers Grove, IL). The biodistribution of ^{68}Ga-GP or ^{18}F-FDG in each sample was calculated as a percentage of the injected dose per gram of the tissue's wet weight (%ID/g).

2.5. MIRD Dosimetry Estimates. Rat absorbed doses estimates for ^{68}Ga-GP were computed from their respective biodistribution data. Fitted residence time functions were plotted and multiplied by the exponential decay functions (i.e., half-life) for ^{68}Ga-GP. These functions were then integrated analytically to determine the area under the curve (AUC) to yield the residence time of each organ. It was assumed that the injected activity distribution was uniformly distributed throughout the body immediately following injection. It was further assumed that no excretion occurred after the last time point and that the activity distribution remained unchanged after this time point; that is, no biological excretion was assumed after the last time point. Mass correction factors were used to account for the different ratios of organ to total body weights in the rat and in humans and allowed for the scaling of the rat residence times to human residence times. For the organs where total organ weight was unavailable, the organ weights derived from the Cristy-Eckerman mathematic phantoms for the adult male were used to estimate total tissue activity. Residence times were then used to calculate target organ absorbed radiation doses with *S*-value tables for a standard 70 kg male model using the MIRDose Olinda software package (Oakridge, TN). Each organ dose was computed from the sum of self-dose plus the dose it received from each source organ in

Table 3: Radiation dose estimates of reference adult for ^{68}Ga-GP from rabbits.

Organs (5 rem annual/15 rem total)			
Target organ	rad/mCi	Human dose (mCi)	rad
adrenals	2.54*E*− 04	20	0.005
brain	7.37*E*− 06	20	0.000
breasts	2.78*E*− 04	20	0.006
gall bladder wall	1.03*E*− 04	20	0.002
lli wall	8.24*E*− 06	20	0.000
small int	2.34*E*− 05	20	0.000
stomach	1.69*E*− 04	20	0.003
uli wall	3.02*E*− 05	20	0.001
heart wall	2.30*E*− 02	20	0.460
kidneys	7.92*E*− 05	20	0.002
liver	2.13*E*− 04	20	0.004
lungs	4.62*E*− 04	20	0.009
muscle	9.27*E*− 05	20	0.002
pancreas	2.54*E*− 04	20	0.005
bone surfaces	8.54*E*− 05	20	0.002
skin	4.65*E*− 05	20	0.001
testes	2.09*E*− 06	20	0.000
thymus	8.81*E*− 04	20	0.018
thyroid	5.34*E*− 05	20	0.001
urine bladder wall	5.92*E*− 06	20	0.000
uterus	1.11*E*− 05	20	0.000
eff dose	1.48*E*− 04	20	0.003
Blood-forming organs (3 rem annual/5 rem total)			
ovaries	1.16*E*− 05	20	0.000
red marrow	1.29*E*− 04	20	0.003
spleen	1.18*E*− 04	20	0.002
eff dose eq	1.60*E*− 03	20	0.032
total body	1.92*E*− 04	20	0.004

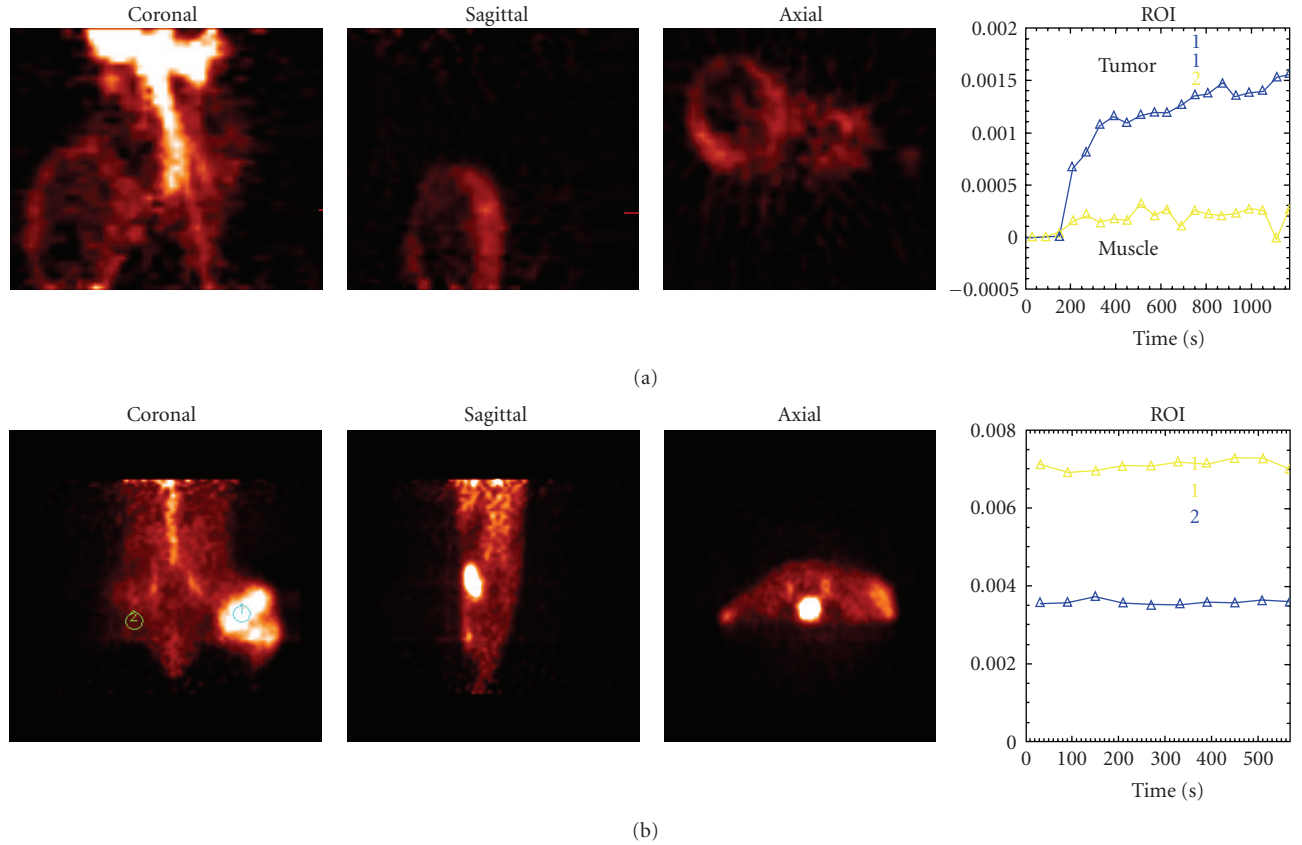

Figure 5: Dynamic mPET Imaging of ^{68}Ga-GP (a) and ^{18}F-FDG (b) in breast tumor bearing rats (0.003 mg, 600 uCi/rat, iv) at 0–20 min showed tumor could be visualized by both compounds.

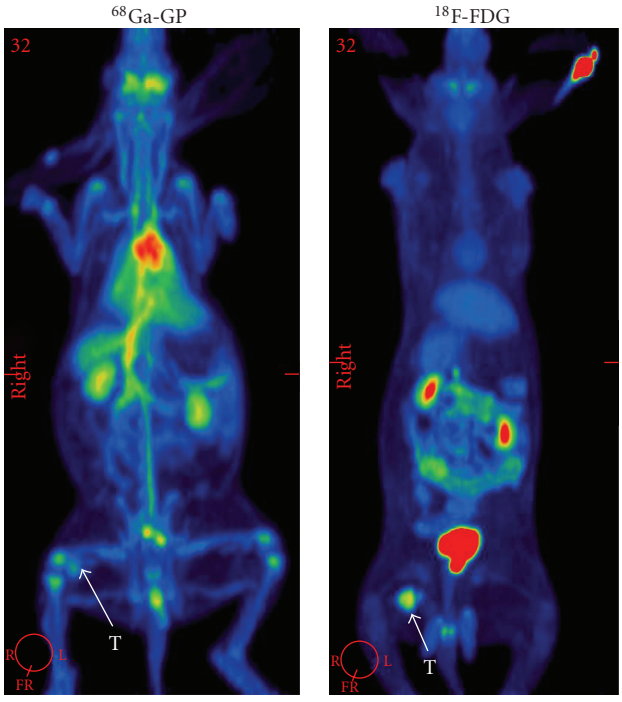

Figure 6: PET whole body at 45 min in New Zealand white rabbits bearing VX2 tumors.

the body or from the remainder of the body. The estimated human radiation absorption dose was determined.

2.6. PET Imaging Studies. For microPET imaging, the images were acquired on a microPET R4 scanner, a dedicated 3D small-animal PET (Concorde Microsystems, Knoxville TN). A group of female Fischer 344 tumor-bearing rats was injected intravenously with ^{68}Ga-GP or ^{18}F-FDG ($n = 3$ rats/compound) through the tail veins. Each animal will be anesthetized and secured onto the microPET. Cradle notches, laser lights, and animal felt pen markings will be used to ensure reproducible animal positioning before and after administration of ^{68}Ga-GP and ^{18}F-FDG. Each animal will then be injected with 1.62 μCi/g body weight of ^{68}Ga-GP and ^{18}F-FDG and imaged for 2 hr in a dynamic mode. A minimum of ~20 million events will be acquired in 120 minutes covering the tumor bearing area. The acquired list mode data will then be histogramed into frames of varying durations using Fourier rebinning. The corresponding images will be reconstructed into 128∗128∗63(0.72∗0.72∗1.3 mm) matrix using ordered subset expectation maximization techniques. All corrections for attenuation, scatter, dead-time, and randomizations were applied to generate quantifiable images. Computer-outlined region of interest (counts per pixel) of the tumor and muscle (at the symmetric site) was used to determine tumor-to-muscle count density ratios.

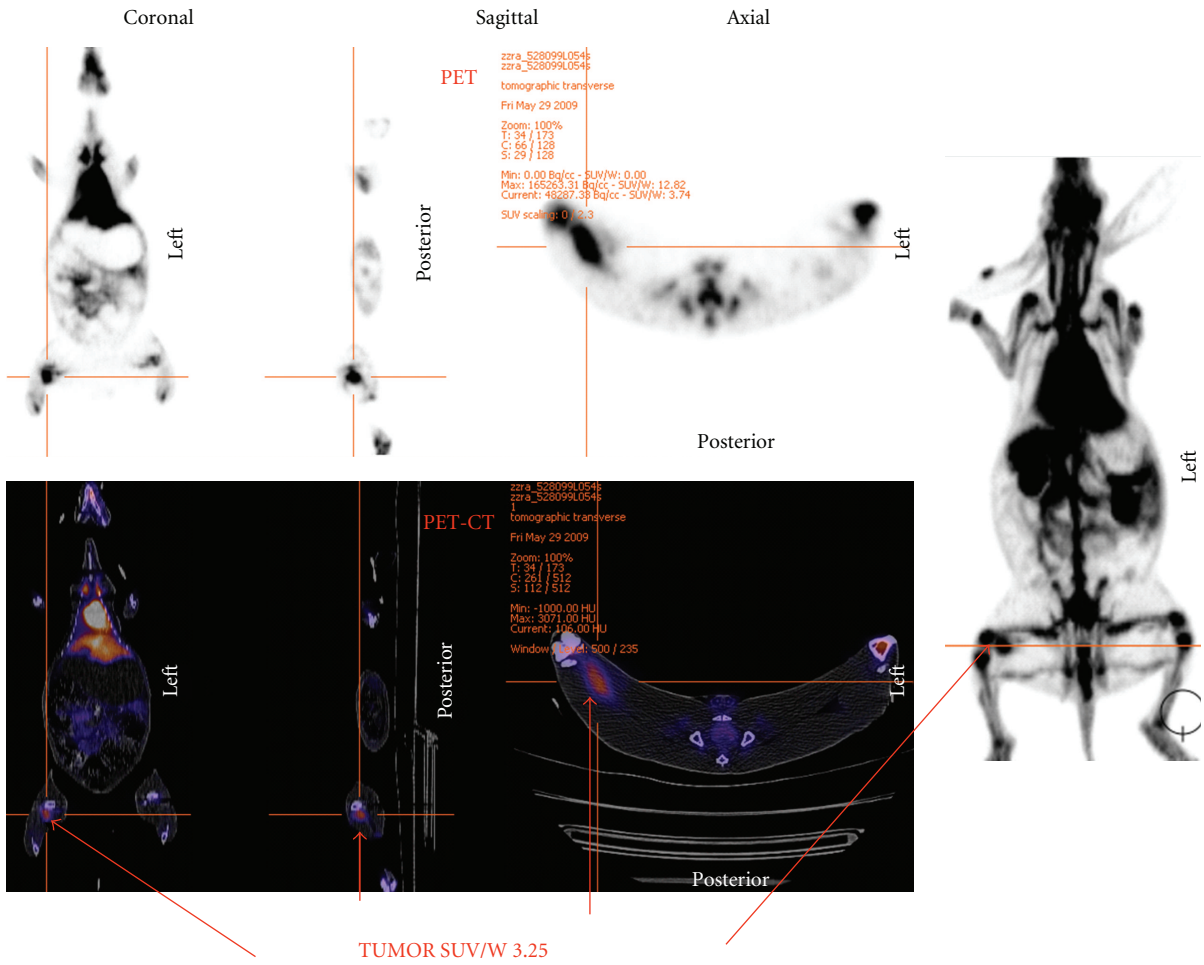

FIGURE 7: 45 minutes dynamic image with PET-CT of ^{68}Ga-GP in a New Zealand white rabbit bearing VX2 tumor showed SUV of the tumor was 3.25.

For PET/CT imaging in large animals, New Zealand white rabbits were inoculated with VX-2 tumor mass (rabbit-driven squamous tumors). The rabbits were administered intravenously (iv) 2 mCi of ^{68}Ga-GP and ^{18}F-FDG (control). The images were acquired on a dedicated Advance 3D PET/CT (GE Medical system) at 0.5–2 hr after i.v. injection of the radiotracers. Standard uptake value of tumors was determined by dynamic PET up to 45 min.

2.7. Kinetic Study of Blood Clearance of ^{68}Ga-GP in New Zealand White Rabbit. New Zealand white rabbits were administered intravenously (iv) 2 mCi of ^{68}Ga-GP. To determine blood clearance and half-life of ^{68}Ga-GP, 0.1 ml blood samples were collected from 10 seconds to 20 min (14 time points) after injection. Blood samples were weighted, and the radioactivities were counted by gamma counter (Packard Instruments, Downers Grove, IL). The radioactivity of each sample was calculated as a percentage of the injected dose per gram of the blood's net weight (%ID/g).

3. Results

3.1. Chemistry. Elemental analysis of GP ($C_{11}H_{14}N_2Na_2O_6$, C, H, N) showed C: 41.54, H: 10 : 62, and N: 7.19. (calculated C: 41.77, H: 8.86, and N: 4.43). The estimated purity of GP was greater than 95% (based upon carbon content). Gel permeation chromatogram (GPC) and capillary electrophoresis (CE) spectra showed that the purity of GP was greater than 95% (Figures 2 and 3). From radio-TLC (Bioscan, Washington, DC) analysis, the radiochemical purity was more than 95% (Rf = 0.1). In vitro stability assays indicated that the radiation yield is 98.67% at 30 min and 97.73% at 2 hr after labeling. There was no breakdown ^{68}Ga-GP up to 2 hr (Figure 4).

3.2. Biodistribution Studies. There was an increased uptake in tumors (percent of injected dose per gram of tissue), tumor-to-blood and tumor-to-muscle count density ratios by ^{68}Ga-GP at 0.5–2 hr, whereas the optimum tumor uptake and tumor-to-muscle count density ratios for ^{18}F-FDG were at 1 hr after administrations (Tables 1 and 2). In biodistribution

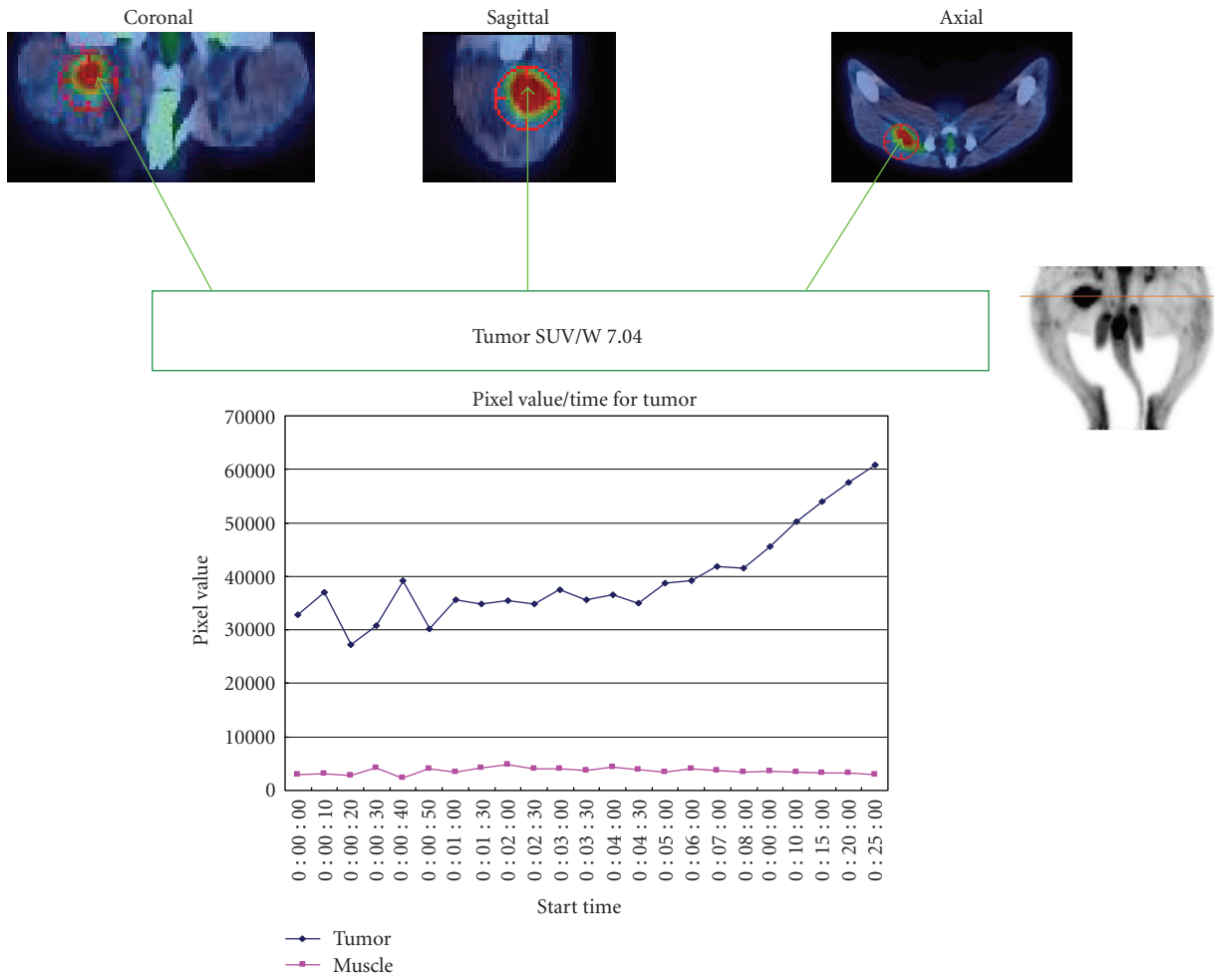

Figure 8: 45 minutes dynamic image with PET-CT of ^{18}FDG in New Zealand white rabbit bearing VX2 tumor showed SUV of the tumor was 7.04.

studies at 30, 60, and 120 min, tumor uptake values, tumor/blood, and tumor/muscle ratios for ^{68}Ga-GP were 0.68 ± 0.12 to 1.18 ± 0.09, 0.26 ± 0.03 to 0.86 ± 0.09, and 6.12 ± 1.87 to 13.26 ± 4.41 and for ^{18}F-FDG were 2.03 ± 0.18 to 2.49 ± 0.08, 5.19 ± 0.38 to 34.37 ± 1.76, and 2.87 ± 0.24 to 7.54 ± 0.56, respectively (Tables 1 and 2).

3.3. MIRD Dosimetry Estimates. The rabbit imaging data was used to calculate residence times for each organ through analytical integration. The residence times were scaled from rabbit to human (70 kg reference adult model) using organ correction factors to generate human residence time estimates. The kidneys and spleen are the primary and secondary contributors for ^{68}Ga-GP, respectively. The MIRD output was multiplied by a proposed human dose of 20 mCi for ^{68}Ga-GP to yield total absorbed dose shown in Table 3. ^{68}Ga-GP showed total rad absorbed by each organ was below the proposed annual and total limits. Radiation exposure to the whole body, blood-forming organs (red marrow and spleen), gonads (testes and ovaries), and effective dose equivalent for the proposed human single dose at 20 mCi fall below the limits of 3 rad annually and 5 rad total. The absorbed dose in all other organs (e.g., kidneys) was below the limits of single dose of 5 rad annually and 15 rad total (Table 3). These radiation exposure values are commonly accepted as criteria for in vivo radiation safety measurement.

3.4. PET Imaging Studies. Tumors could be well visualized both in breast tumor-bearing rats and VX-2 tumor-bearing rabbits (Figures 5 and 6). From PET image ROI analysis, standard tumor uptake values (SUVs) for ^{68}Ga-GP and ^{18}F-FDG in VX-2 tumor-bearing rabbits were 3.25 and 7.04, respectively (Figures 7 and 8). PET images in tumor-bearing rats and rabbits confirmed that ^{68}Ga-GP could assess tumor uptake. PET dynamic scan showed fast tumor uptake of ^{68}Ga-GP in a New Zealand white rabbit bearing VX2 tumor (Figure 9). Furthermore, there is no intestine uptake in ^{68}Ga-GP PET imaging indicated the radioisotope labeling of ^{68}Ga-GP is stable *in vivo*.

3.5. Kinetic Study of Blood Clearance of ^{68}Ga-GP in New Zealand White Rabbit. The blood clearance of ^{68}Ga-GP showed both distribution phase and elimination phase (Figure 10(a)). The elimination phase was used to calculate

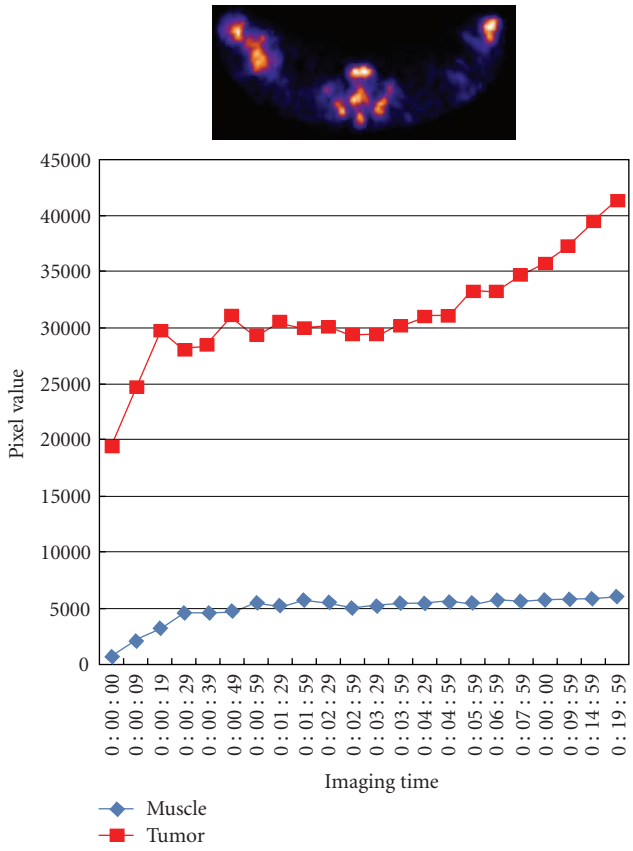

FIGURE 9: 45 Minutes dynamic tumor uptake of ^{68}Ga-GP in a New Zealand white rabbit bearing VX2 tumor. The axial view from PET-CT showed the location of tumor.

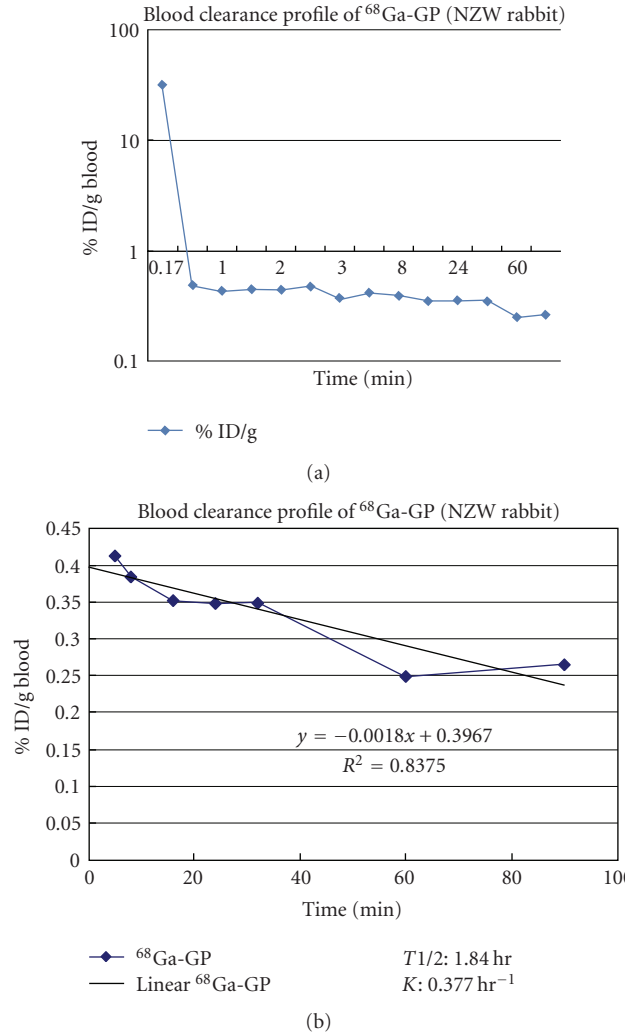

FIGURE 10: Blood clearance (a) and half-life analysis (one compartment) of ^{68}Ga showed the half-life of ^{68}Ga-GP was 1.84 hr with K value of 0.377 hr.

the half-life ($T1/2$) of ^{68}Ga-GP (Figure 10(b)). Regression line formulation ($y = -0.0018x + 0.3967$, $R^2 = 0.8375$) was estimated using Microsoft Office Excel 2003. The $T1/2$ of ^{68}Ga-GP was 1.84 hr and the elimination rate constant (k) was 0.377 hr^{-1}.

4. Discussion

Chitosan, a cationic biopolymer derived by deacetylation of chitin. Chitin and chitosan derivatives are used as excipients and drug carriers in the pharmaceutical field. For instance, films prepared using chitin or chitosan have been developed as wound dressings, oral mucoadhesive, and water-resisting adhesive by virtue of their release characteristics and adhesion. Intratumoral administration of gadopentetic acid-chitosan complex nanoparticles (approximately 430 nm in diameter) has been more effective for gadolinium neutron-capture therapy compared with a group treated with the solution. Chitin and chitosan derivatization contributed to expansion of application in drug delivery and sustained drug release [12–14]. It has been reported that chitosan could directly conjugate drugs or be modified by the introduction of thioglycolic acid (TGA) resulting in chitosan-TGA conjugates with thiol groups. Chitosan-thioglycolic acid conjugates has been found to be a promising candidate in tissue engineering due to their physicochemical properties [15]. Despite the broadened application of chitosan derivatives, one major limitation of chitosan is lack of cellular targeting.

Previous studies have shown that glutamate peptide is a candidate of drug carrier [16, 17]. Radiolabeled glutamic acid has shown to be useful in tumor cellular imaging [18]. To optimize the intracellular uptake of chitosan derivatives, we have synthesized glutamate peptide, chitosan, and a GP copolymer. This copolymer would be ideal to conjugate the drugs with either amino or acid groups which provides an advantage over either chitosan or glutamate peptide. In addition, results from our previous in vitro cellular uptake and animal imaging studies showed that GP is a target drug carrier via glutamate transporters [10]. This targeted drug carrier may provide an advantage not only to improve drug solubility but also to overcome drug resistance during chemotherapy.

In our previous findings, ^{99m}Tc-GP was able to measure uptake differences after cells treated with paclitaxel and

uptake difference between tumor and inflammation. In vitro cellular uptake assay indicated that cellular uptake of ^{99m}Tc-GP was via glutamate transporters. In this study, we further tested the ^{68}Ga-GP imaging using PET/CT.

In summary, PET imaging studies indicated that it is feasible to use ^{68}Ga-GP to image tumors. GP has multiamino and acid groups which broaden its chemistry application.

5. Relevance

At present, there is no angiogenesis imaging agent focused on both vascular endothelial adhesiveness and cellular targets. GP interacts with vascular endothelial and cellular targets. GP also has multiple amino and carboxylic groups, which allows anticancer drug conjugate for targeted imaging and therapy. Our data indicate that ^{68}Ga-GP accumulates actively in tumors both in small and large animal models (Figures 4 and 5). The imaging data obtained from ^{68}Ga-GP not only provide an impact on improving the diagnosis of cancer but also provide a basis for internal radionuclide targeted therapy.

Acknowledgments

This work was supported in part by a generous gift from Taiwan Hopax Chems, MFG, Co., Ltd (Taiwan). The animal research is supported by M. D. Anderson Cancer Center (CORE) Grant no. NIH CA-16672.

References

[1] F. Bertolini, M. Paolucci, F. Peccatori et al., "Angiogenic growth factors and endostatin in non-Hodgkin's lymphoma," *British Journal of Haematology*, vol. 106, no. 2, pp. 504–509, 1999.

[2] Y. Cao, "Therapeutic potentials of angiostatin in the treatment of cancer," *Haematologica*, vol. 84, no. 7, pp. 643–650, 1999.

[3] B. D. Smith, G. L. Smith, D. Carter, C. T. Sasaki, and B. G. Haffty, "Prognostic significance of vascular endothelial growth factor protein levels in oral and oropharyngeal squamous cell carcinoma," *Journal of Clinical Oncology*, vol. 18, no. 10, pp. 2046–2052, 2000.

[4] T. Mori, M. Okumura, M. Matsuura et al., "Effects of chitin and its derivatives on the proliferation and cytokine production of fibroblasts in vitro," *Biomaterials*, vol. 18, no. 13, pp. 947–951, 1997.

[5] A. Polykratis, P. Katsoris, J. Courty, and E. Papadimitriou, "Characterization of heparin affin regulatory peptide signaling in human endothelial cells," *Journal of Biological Chemistry*, vol. 280, no. 23, pp. 22454–22461, 2005.

[6] J. S. Pieper, P. B. Van Wachem, M. J. A. Van Luyn et al., "Attachment of glycosaminoglycans to collagenous matrices modulates the tissue response in rats," *Biomaterials*, vol. 21, no. 16, pp. 1689–1699, 2000.

[7] R. A. Waniewski and D. L. Martin, "Characterization of L-glutamic acid transport by glioma cells in culture: evidence for sodium-independent, chloride-dependent high affinity influx," *Journal of Neuroscience*, vol. 4, no. 9, pp. 2237–2246, 1984.

[8] C. Chenu, C. M. Serre, C. Raynal, B. Burt-Pichat, and P. D. Delmas, "Glutamate receptors are expressed by bone cells and are involved in bone resorption," *Bone*, vol. 22, no. 4, pp. 295–299, 1998.

[9] M. Béhé, G. Kluge, W. Becker, M. Gotthardt, and T. M. Behr, "Use of polyglutamic acids to reduce uptake of radiometal-labeled minigastrin in the kidneys," *Journal of Nuclear Medicine*, vol. 46, no. 6, pp. 1012–1015, 2005.

[10] I. C. Wei, N. Tsao, YA. H. Huang et al., "^{99m}Tc-glycopeptide: synthesis, biodistribution and imaging in breast tumor-bearing rodents," *Applied Radiation and Isotopes*, vol. 66, no. 3, pp. 320–331, 2008.

[11] S. Froidevaux, M. Calame-Christe, J. Schuhmacher et al., "A gallium-labeled DOTA-α-melanocyte-stimulating hormone analog for PET imaging of melanoma metastases," *Journal of Nuclear Medicine*, vol. 45, no. 1, pp. 116–123, 2004.

[12] L. Y. Wang, G. H. Ma, and Z. G. Su, "Preparation of uniform sized chitosan microspheres by membrane emulsification technique and application as a carrier of protein drug," *Journal of Controlled Release*, vol. 106, no. 1-2, pp. 62–75, 2005.

[13] M. Fujita, M. Ishihara, Y. Morimoto et al., "Efficacy of photocrosslinkable chitosan hydrogel containing fibroblast growth factor-2 in a rabbit model of chronic myocardial infarction," *Journal of Surgical Research*, vol. 126, no. 1, pp. 27–33, 2005.

[14] Y. Kato, H. Onishi, and Y. Machida, "Application of chitin and chitosan derivatives in the pharmaceutical field," *Current Pharmaceutical Biotechnology*, vol. 4, no. 5, pp. 303–309, 2003.

[15] A. Bernkop-Schnürch, M. Hornof, and D. Guggi, "Thiolated chitosans," *European Journal of Pharmaceutics and Biopharmaceutics*, vol. 57, no. 1, pp. 9–17, 2004.

[16] D. J. Yang, C. Li, S. Nikiforow et al., "Diagnostic and therapeutic potential of poly(benzyl L-glutamate)," *Journal of Pharmaceutical Sciences*, vol. 83, no. 3, pp. 326–331, 1994.

[17] W. Tansey, S. Ke, X. Y. Cao, M. J. Pasuelo, S. Wallace, and C. Li, "Synthesis and characterization of branched poly(L-glutamic acid) as a biodegradable drug carrier," *Journal of Controlled Release*, vol. 94, no. 1, pp. 39–51, 2004.

[18] R. E. Reiman, R. S. Benua, and A. S. Gelbard, "Imaging of brain tumors after administration of L-(N-13)glutamate: concise communication," *Journal of Nuclear Medicine*, vol. 23, no. 8, pp. 682–687, 1982.